Increase in tracheal investment with beetle size supports hypothesis of oxygen limitation on insect gigantism

Alexander Kaiser*†, C. Jaco Klok‡, John J. Socha§, Wah-Keat Lee§, Michael C. Quinlan*, and Jon F. Harrison‡

*Department of Basic Sciences, Midwestern University, Glendale, AZ 85308; ‡Section of Organismal, Integrative and Systems Biology, School of Life Sciences, Arizona State University, Tempe, AZ 85287-4501; and §X-Ray Science Division, Advanced Photon Source, Argonne National Laboratory, Argonne, IL 60439

Edited by May R. Berenbaum, University of Illinois at Urbana–Champaign, Urbana, IL, and approved July 5, 2007 (received for review December 24, 2006)

Recent studies have suggested that Paleozoic hyperoxia enabled animal gigantism, and the subsequent hypoxia drove a reduction in animal size. This evolutionary hypothesis depends on the argument that gas exchange in many invertebrates and skin-breathing vertebrates becomes compromised at large sizes because of distance effects on diffusion. In contrast to vertebrates, which use respiratory and circulatory systems in series, gas exchange in insects is almost exclusively determined by the tracheal system, providing a particularly suitable model to investigate possible limitations of oxygen delivery on size. In this study, we used synchrotron x-ray phase–contrast imaging to visualize the tracheal system and quantify its dimensions in four species of darkling beetles varying in mass by 3 orders of magnitude. We document that, in striking contrast to the pattern observed in vertebrates, larger insects devote a greater fraction of their body to the respiratory system, as tracheal volume scaled with mass$^{1.29}$. The trend is greatest in the legs; the cross-sectional area of the trachea penetrating the leg orifice scaled with mass$^{1.02}$, whereas the cross-sectional area of the leg orifice scaled with mass$^{0.77}$. These trends suggest the space available for tracheae within the leg may ultimately limit the maximum size of extant beetles. Because the size of the tracheal system can be reduced when oxygen supply is increased, hyperoxia, as occurred during late Carboniferous and early Permian, may have facilitated the evolution of giant insects by allowing limbs to reach larger sizes before the tracheal system became limited by spatial constraints.

allometric scaling | hyperoxia | Tenebrionidae | tracheal system

The mechanisms responsible for limitations on animal size are generally unknown. Recent high-profile publications have suggested that the atmospheric oxygen partial pressure (aPO_2) provides a key biophysical limitation on the maximal size of some animal groups, and specifically that elevations in aPO_2 increased oxygen supply to the tissues, allowing larger body sizes (1, 2). According to this oxygen-limitation hypothesis, high aPO_2 values near 30 kPa in the late Carboniferous and early Permian led to the evolution of giant organisms in many animal groups (1, 2). The subsequent aPO_2 decrease in the Triassic resulted in lower gas transfer rates and in substantially smaller body sizes of the surviving fauna of these groups (2). A corollary of this hypothesis is that the present 20.9-kPa level of aPO_2 prevents extant descendants from becoming giants again. The oxygen-limitation hypothesis has been widely publicized, but empirical support for a specific mechanism by which changes in aPO_2 can influence the maximal body size for animals is lacking.

Regardless of whether gas transport occurs by diffusion or convection, the amount of gas transported through an exchanging structure is directly proportional to the cross-sectional area of the structure and the partial pressure difference of the gas but is inversely related to the distance from atmosphere to tissues. The larger an animal grows, the greater is the distance for respiratory gas transport, but we know little about how volume or cross-sectional area of gas transport systems varied with size in animals that experienced Paleozoic gigantism. As yet, techniques have not been refined to examine the dimensions of the respiratory system in fossils of extinct animals. We can, however, investigate whether scaling of oxygen supplying structures in the existing fauna explains size limits at the current atmospheric oxygen level.

Insects are excellent model organisms to test the oxygen-limitation hypothesis. They were one of the major animal groups that experienced gigantism in the late Paleozoic (3), and their respiratory system is relatively simple. Air-filled tracheal tubes transport oxygen to the tissues. The circulatory system contributes little to oxygen transport, because the capacitance of hemolymph for oxygen is low. In contrast, most gill- and lung-breathing animals must operate respiratory and circulatory systems in series to deliver oxygen. Gills and circulatory systems, however, fulfill more functions than gas exchange, such as ion regulation in the gills or transport of nutrients in the circulatory system, complicating analyses of scaling.

In theory, morphological dimensions of the tracheal system could increase with body mass with three scaling patterns (4, 5).

(*i*) Larger insects could invest a smaller fraction of their body in the tracheal system (negative allometry; ref. 5). Volume measures (e.g., tracheal or air sac volumes) would scale with body mass with a scaling coefficient <1, and cross-sectional areas would scale with mass with a scaling coefficient <0.67. The fraction of the body volume occupied by tracheae in larger insects might decrease, because mass-specific metabolic rate and oxygen demand decrease with size in most organisms, including tracheated arthropods (6, 7). Many scaling coefficients of gills and skin, which are gas exchange surfaces for aquatic animals, can be explained by lower mass-specific metabolic rates in larger animals (8–11). In some skin-breathing vertebrates, reduced surface-to-volume ratio leads to increased critical PO_2 values for oxygen uptake in larger animals, potentially limiting body size (10).

(*ii*) Larger insects could invest a greater fraction of their body in the tracheal system (positive allometry; ref. 5). The scaling coefficient would be >1 for tracheal volumes and >0.67 for tracheal cross-sectional areas. Larger insects might need to devote a greater fraction of their body to tracheae if increased distances for oxygen delivery require increased respiratory in-

Author contributions: A.K., M.C.Q., and J.F.H. designed research; A.K., C.J.K., J.J.S., W.-K.L., and J.F.H. performed research; J.J.S. and W.-K.L. contributed new reagents/analytic tools; A.K. analyzed data; and A.K., C.J.K., J.J.S., W.-K.L., M.C.Q., and J.F.H. wrote the paper.

The authors declare no conflict of interest.

This article is a PNAS Direct Submission.

Abbreviations: aPO_2, atmospheric oxygen partial pressure; SMA, standard major axis; PIC, phylogenetically independent contrast.

†To whom correspondence should be addressed. E-mail: akaise@midwestern.edu.

This article contains supporting information online at www.pnas.org/cgi/content/full/0611544104/DC1.

vestment. To our knowledge, this scaling pattern has not been demonstrated for the respiratory system in any interspecific comparison of adults from any animal group. The increased investment in tracheal volumes (12) and tracheolar densities (13) in larger or older grasshoppers and proportionally larger lung dimensions in rats, mice, and infants postpartum (14–16) suggest that positive allometric growth may occur during development. An increasing fractional volume of the respiratory system in larger animals could limit maximal body size, by reducing the space for other tissues.

(*iii*) Larger insects could invest the same fraction of body volume in the tracheal system (isometry; ref. 5). This pattern would be indicated by scaling coefficients not significantly different from 1 for tracheal volume and not significantly different from 0.67 for tracheal cross-sectional areas. Organ masses and volumes, such as the heart and lung, tend to exhibit isometry in adult vertebrates (17–19). Isometric scaling would not limit body size. Authors generally treat isometry as the default expectation for mass-specific scaling of tissues but do not attempt to provide functional explanations. One functional hypothesis to explain isometric scaling of respiratory structures in tracheated arthropods is that decreasing mass-specific oxygen demand and increasing length of oxygen transport pathways act as counterbalancing effects. We treat isometry as the null hypothesis for scaling of the tracheal system of adult tenebrionid beetles.

Recent studies have shown that growing grasshoppers increase mass-specific tracheal volumes, diffusing capacities, and tidal volumes after each molt (4, 12, 13). These ontogenetic changes, however, are not necessarily related to size *per se* but may be related to developmental changes, such as the ability to fly (ref. 5; ontogenetic allometry). Thus it is necessary to investigate interspecific scaling among adult insects to understand the morphological bases of evolutionary limits of body size (ref. 5; static and phylogenetic allometry).

We examined tracheal investment patterns of 44 individuals from four species of darkling beetles (Coleoptera: Tenebrionidae) spanning 3 orders of magnitude in body mass (1.6–1,700 mg) and 1 order of magnitude in body length (3.2–33 mm). To visualize the tracheal system of living animals we used synchrotron x-ray phase-contrast imaging (20). We analyzed tracheal volumes in x-ray images with the stereological point count method for histological sections (21). We modified the method to account for the overlap of tracheae within a 3D structure [supporting information (SI) Figs. 5 and 6]. Oxygen must be transported to the head and the legs, but these structures lack spiracles in insects (Fig. 1); in tenebrionid beetles, the head is supplied via thoracic spiracles (Fig. 1, mss) and the legs via thoracic and abdominal spiracles (Fig. 1, mss, mts, and a1). As a consequence, the distances for oxygen delivery to these tissues are long, and the supplying tracheae must cross the potential bottlenecks of the exoskeletal orifices of the head capsule (Fig. 1, ht) and the first (coxal) leg segment (Fig. 1, cxt; Fig. 2). Therefore, we examined whether the space available for tracheae within these structures might represent a possible morphological limitation to body size by measuring cross-sectional areas of orifices and penetrating tracheae.

We tested each variable against the null hypothesis of isometry; slopes of 1 for log volume vs. log mass regressions and slopes of 0.67 for log cross-sectional area vs. log mass regressions. We used the standard major axis (SMA) line-fit (22) on phylogenetically independent contrasts (PIC) (23). Phylogenetic correction was based on the combination of two phylogenetic trees with branch lengths normalized by tree length (figure 49, ref. 24; ref. 25). We show that, in contrast to vertebrates, larger beetles invest more in the gas exchange system, and we present a model that demonstrates how space available for tracheae, especially within the leg orifice, may lead to oxygen limitation of body size in this group.

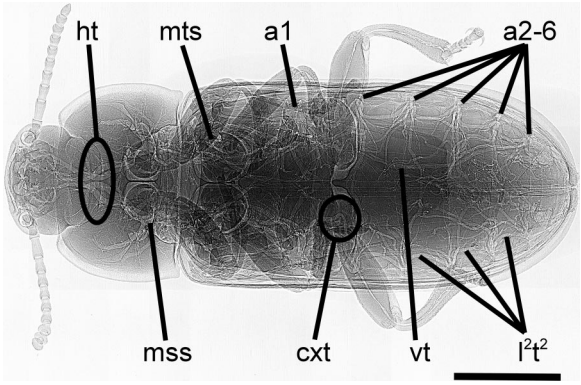

Fig. 1. X-ray image of the tenebrionid beetle *T. molitor*. The body is divided into head, first thoracic segment, and fusion of two thoracic and all abdominal segments, which is covered by hardened front wings. The head is supplied by four major head tracheae (ht) branching pair-wise from the two mesothoracic spiracles (mss). The three pairs of thoracic legs are supplied with air via a coxal trachea (cxt) through the mesothoracic (mss), the metathoracic (mts), and the first abdominal spiracles (a1). Lateral longitudinal tracheal trunks (l^2t^2) connect all spiracles on one side. Visceral tracheae (vt) extend from the abdominal spiracles (a1, a2–6) into the abdomen. In every segment, a transverse tracheal branch connects left and right manifolds. Air sacs are absent in all species. ht and cxt are regions where we investigated scaling of exoskeletal orifices and penetrating tracheal tubes. Body anatomy and tracheal system morphology is similar for all four species. (Scale bar, 2 mm.)

Results and Discussion

The general organization and structure of the tracheal system were similar in all four species (Fig. 1). In striking contrast to the scaling pattern observed in vertebrates, larger beetles devote a greater fraction of their body volume to gas exchange structures. Whole-body tracheal volume increased with a mass-scaling coefficient of 1.29 (Table 1), with tracheal volumes increasing from 0.5% in the smallest species, *Tribolium castaneum*, to 4.8% in *Eleodes obscura*, the largest species we examined (Fig. 3*A*). Regional analyses of cross-sectional areas indicated that the leg trachea occupied a greater proportion of space in the leg orifice in larger beetle species (Fig. 2). The scaling coefficient of tracheae penetrating the leg orifice was 1.02 (Table 1), significantly higher than the 0.67 predicted by isometry, whereas the orifice itself had a scaling coefficient of 0.77 (Fig. 3*C*). The leg tracheal tube in the smallest species occupied only 2% of the leg orifice, whereas 18% was occupied in the largest species. Positive allometry was not evident in the head orifice (Fig. 3*B*); instead, cross-sectional areas of head tracheae and of head orifice scaled isometrically (Table 1). Statistical analyses of species mean data were insensitive to tree structure and branch lengths used for phylogenetic correction (SI Table 2 *A* and *B*) or to line-fit method (SI Table 2*C*). Omitting the phylogenetic correction resulted in marginally lower slopes (SI Table 2 *D* and *E*). The individual data points follow the same trend as the species means (Fig. 3, small circles), demonstrating that intra- as well as interspecific comparisons indicate a greater proportional investment in the tracheal system of larger beetles (SI Table 2*F*).

The increased fraction of the body volume occupied by tracheae in larger insects may compensate for distance effects on diffusive and convective oxygen delivery. Critical PO_2 values do not correlate with body size across insect species or with ontogeny in resting or jumping grasshoppers (26–28). In feeding caterpillars (29) and juvenile grasshoppers (30), critical PO_2 values increase within an instar but not across instars at similar stages, suggesting that feeding and growing tissues reduce tra-

PHYSIOLOGY

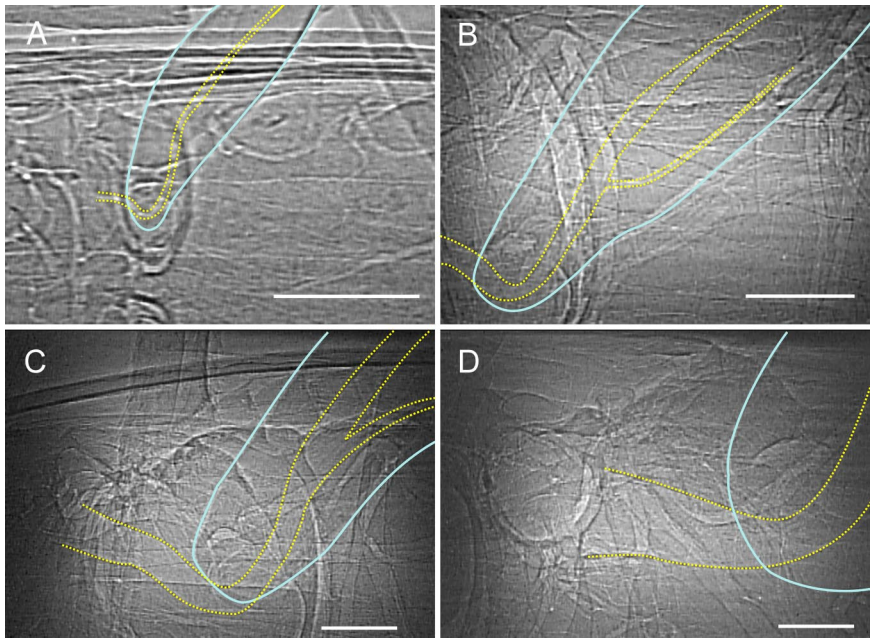

Fig. 2. X-ray images of metathoracic legs and parts of the thorax of four tenebrionid beetle species. Images are arranged in order of increasing body size. (*A*) *T. castaneum* (2.0 ± 0.3 mg); (*B*) *T. molitor* (132.2 ± 20.2 mg); (*C*) *E. armata* (688.6 ± 340.6 mg); (*D*) *E. obscura* (1,350.0 ± 255.0 mg). Images are dorsoventral views, with anterior to the left. Second segments of the leg (femur) are outlined with solid blue lines; leg tracheae are outlined with dotted yellow lines. Tracheal investment in the leg increases strongly with body size (Table 1 and Figs. 3 and 4). (Scale bars, 250 μm.)

cheal volume until the molt occurs. Our data support studies that suggest that larger instars and adults are able to maintain critical PO_2 values with size by increasing fractional tracheal dimensions, diffusing capacities, and tidal volumes (4, 12, 13, 29, 30).

If continued unabated, increasing proportional investment in the tracheal system can lead to spatial conflicts within the organism, because the larger respiratory system leaves less space for other tissues. Is the magnitude of this effect consistent with oxygen limitation of size in extant insects? We addressed this question by extrapolating the relationship between relative tracheal densities and body length to limits of tracheal densities found in the literature (Fig. 4). The highest tracheal volume density reported for any insect respiratory system is ≈40% (30–32). If this value represents an upper limit on tracheal volume densities in the body core, the maximal length of darkling beetles would be 32 cm (Fig. 4, TrD_{tot}). Because this estimated body size is much larger than that of any known extant species, this analysis suggests that tracheal investment in the body core does not limit beetle size. In a parallel analysis of the leg, we conservatively estimated that beetles need at least 10% of the coxal orifice area for nerves, tendons, and hemolymph. Under this assumption, our data suggest that no living beetle should be >16 cm (Fig. 4, TrD_{leg}). The largest living beetle is *Titanus giganteus* (Coleoptera: Cerambycidae) with a body length of ≈17 cm (33), suggesting that spatial constraints in the leg limit body size in beetles.

Our discovery that, under the current aPO_2, extant beetles devote greater fractions of their body to the tracheal system, especially in the leg, may provide an explanation for the evolution of gigantic insects under elevated aPO_2 in the Paleozoic. Hyperoxic atmospheres can alter the scaling of the tracheal system in two ways: first, insects could grow larger with longer appendages, because the higher amount of oxygen reduces the distance effects on gas exchange; second, the increased partial pressure of oxygen could lead to the evolution of thinner tracheal tubes. Extant insects do reduce the dimensions of their tracheae when reared in hyperoxic environments (34, 35). Increased oxygen delivery, together with reduced tracheal investment, would have allowed insects to evolve much larger, perhaps giant, bodies before the exoskeleton of the leg constrained the size of the respiratory system.

Table 1. Allometric scaling of tracheal and exoskeletal structures with body mass in four species of tenebrionid beetles

Log body mass (mg) related scaling: Log Y = intercept + slope × log body mass

	Slope	SE	Intercept	r	S_{Hyp}	t_{Hyp}	p_{Hyp}
Log tracheal volume, ml	1.294	0.061	−2.293	0.998	1.0	4.824	0.040
Cross-sectional areas							
Log head orifice, mm²	0.622	0.024	−0.962	0.999	0.67	1.842	0.207
Log head tracheae, mm²	0.783	0.040	−2.798	0.997	0.67	2.909	0.101
Log leg orifice, mm²	0.770	0.062	−2.370	0.993	0.67	1.670	0.237
Log leg trachea, mm²	1.024	0.024	−4.027	0.999	0.67	15.140	0.004

SMA (22) line-fit on phylogenetically independent contrasts (23). Phylogenetic correction to minimize variance of independent contrasts is based on the combination of two phylogenetic trees with branch lengths normalized by tree length (24, 25). SE, standard error of slope; r, Pearson's correlation coefficient; S_{Hyp}, hypothetical slope for the null hypothesis of isometry; t_{Hyp}, t value for comparison of actual and hypothetical slope (40); p_{Hyp}, probability of equal slopes (significance level, 0.05).

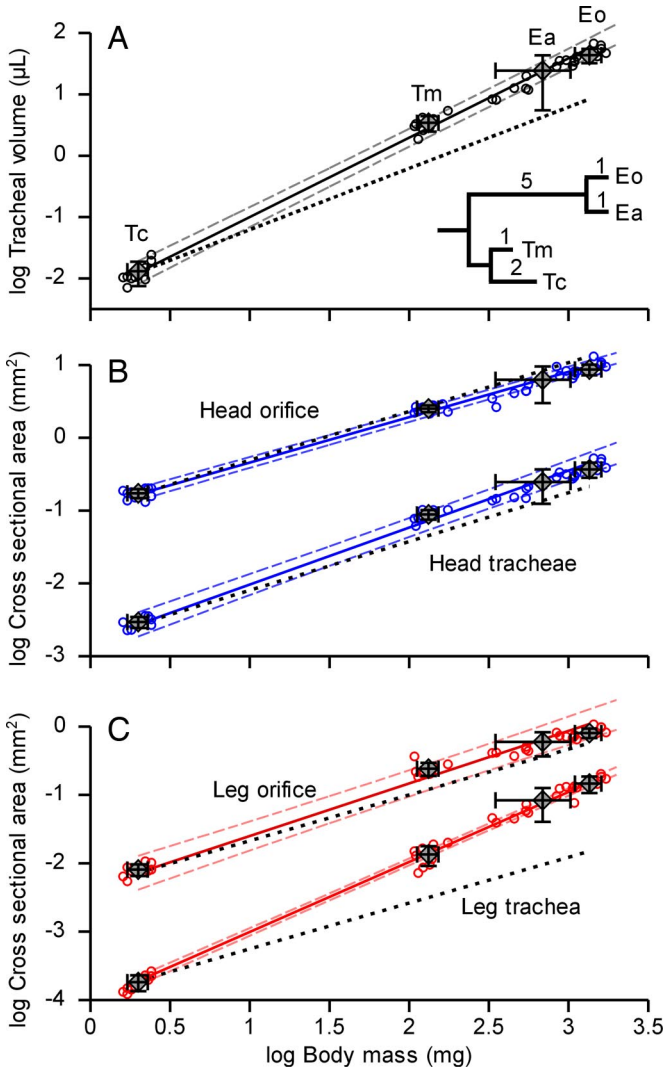

Fig. 3. Scaling of tracheal and exoskeletal structures of four tenebrionid beetle species with body mass. Regression lines (solid lines) were fitted to species mean values ($n = 4$; diamonds, mean ± standard deviation) with the SMA method (22) on PICs (23). Large error bars of *E. armata* (Ea) are due to the large mass range of the measured individuals (ref. 22: ''equation error''); the actual systematic errors are minimal. Individual values (open circles) demonstrate intraspecific scaling that follows interspecific trends. The phylogenetic tree shows hypothesized relationship between species. Branch lengths indicate estimated evolutionary divergence of species (figure 49 of ref. 24; ref. 25). See *Materials and Methods* for details. Eo, *E. obscura*; Tm, *T. molitor*; Tc, *T. castaneum*. Thin dashed lines indicate 95% confidence limits. Black dotted lines indicate isometric slopes. In the whole body and leg, but not the head, beetles devoted a statistically significant increasing fraction of their body to tracheae as they increase in size (see Table 1 for details).

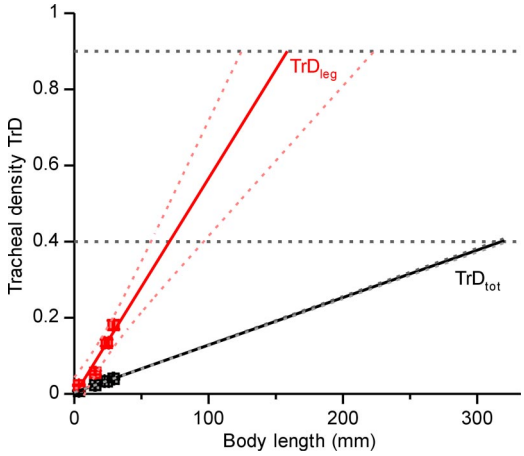

Fig. 4. Estimation of maximum body size in tenebrionid beetles. Proportional tracheal investments in the entire body (TrD_{tot}) and in the leg orifice (TrD_{leg}) of tenebrionid beetles are plotted against body length (mean ± standard error). Line fit (solid lines) was performed by SMA analysis (22) on PICs (23). Dotted lines indicate 95% confidence intervals of line-fit. All slopes are significantly different from 0, indicating increasing tracheal investment with body size. If continued unattenuated, the linear relationship between body length and relative tracheal density in the leg but not in the entire body limits maximum beetle size (dashed lines; see text for details).

$$TrD_{tot} = 0.0037 + 0.001258 \cdot L$$

$$(N = 4;\ r^2 > 0.999;\ p < 0.0001;\ t_0 = 3104;\ p_0 < 0.0001)$$

$$TrD_{leg} = -0.0137 + 0.005902 \cdot L$$

$$(N = 4;\ r^2 = 0.929;\ p = 0.04;\ t_0 = 6.04;\ p_0 = 0.026).$$

Although we do not know the exact point at which spatial constraints will limit insect size, two points are clear from our data. First, larger tenebrionid beetles devote an increasing fraction of their body to tracheae. This trend must impose tradeoffs in spatial allocation with other tissues. Second, model predictions of the maximum size of beetles based on spatial constraints within the leg orifice concur with the size of the largest extant beetle species. This congruence suggests that evolution of giant beetles today would require either higher atmospheric oxygen levels, an attenuation of morphological scaling patterns (5), or a change in the gas exchange mechanism. Our data call for future studies of the scaling of tracheal morphology in the largest extant insect species, as well as in taxa more closely related to those that experienced Paleozoic gigantism.

Materials and Methods

Animals. To compare tracheal structures of darkling beetles (Tenebrionidae), we used adults of four species varying from 3.2 to 33.0 mm in length and from 1.6 to 1,700 mg in mass. *T. castaneum* and *Tenebrio molitor* were purchased from a biological supply company (Carolina Biological Supply, Burlington, NC). *Eleodes armata* was collected in the Mojave Desert near Zzyzx, CA. *E. obscura* was collected in the Sonoran Desert near Phoenix, AZ. All animals were starved for 3 days to minimize acute nutritional variation before the experiments but had free access to water. The two larger species (*E. obscura* and *E. armata*) have reduced hind wings and cannot fly. The other two species (*T. molitor* and *T. castaneum*) possess functional hind wings but usually do not fly.

Image Acquisition and Processing. We analyzed tracheal morphology using synchrotron x-ray phase–contrast imaging (20) at Argonne National Laboratory. Live beetles were immobilized between two layers of x-ray-permeable polyimide film (Kapton; DuPont, Wilmington, DE). We mounted the animals on a stage that could be rotated or translated horizontally or vertically relative to the x-ray beam. Specimens were positioned to obtain a dorsoventral view. Because the field of view (fov) was smaller than the specimens, all beetles were scanned longitudinally from head to telson on one side, back to the head in the center, and again to the telson on the other side. Additionally, the meso- and metathoracic legs of one side (usually the right) were scanned. The x-ray image of the insect was formed on a scintillator screen and reflected onto a CCD video camera (Cohu, San Diego, CA) via a mirror through a microscope objective. Magnification of

PHYSIOLOGY

the camera was ×5 (fov, 1.29 × 0.97 mm) for *T. castaneum* and ×2 (fov, 3.26 × 2.45 mm) for all other beetles. Video sequences were recorded on mini digital video tapes. Video still images were captured by using ATI TV 9.02 software (AMD, Sunny Valley, CA). We optimized digital images by adjusting levels, contrast, and pixel density in Adobe Photoshop (Adobe Systems, San Jose, CA). A 400-mesh copper TEM grid was used for calibration. To obtain dimensions of external structures and the head and leg orifice, we took digital photographs of the body parts with a CCD camera (HVC20M; Hitachi, Brisbane, CA) attached to a stereoscope (Cambridge Instruments; Leica Microsystems, Wetzlar, Germany). A ruler (35-mm length in 0.5-mm steps) was included in the images for calibration. We used Able Image Analyser software (μ-labs, Ljubljana, Slovenia) to measure lengths and areas.

Tracheal Volume Density. X-ray images are 2D projections of a 3D structure. To obtain values for tracheal volume, we used the stereological point count method (21). In this procedure, images were overlaid with a grid of points. The number of points covering the structure relative to the number of total points in the grid is a function of the volume density of the structure (21) (SI Figs. 5 and 6). This method is well established in mammal histology and has been successfully used to determine tracheal dimensions in ultrathin sections of insect tissues (36).

We analyzed the following regions of interest: one side of the head; one side of the pronotum; one mesothoracic spiracle; a second, fourth, and sixth abdominal spiracle with tracheal manifolds; major tracheal branches; and the center of the abdomen. In sum, we measured ≈90% of one body side. Probability errors for volume densities were <5% (21).

Because x-ray images are 2D projections through the body, most images included overlapping tracheae. To compensate, we multiplied each point by the number of tracheal tubes it covered. We converted these projected areas into tracheal volume densities (Fig. 4, TrD_{tot}) by dividing the projection area density by the number of layers of tracheal tubes that could be stacked vertically within a beetle (21). We determined the number of layers by dividing the height of the body part where the image was taken by the mean diameter of the large tracheal branches (SI Fig. 6). Total tracheal volume was calculated by multiplying beetle volume with tracheal volume density. We calculated the total volume of a beetle by summing the volumes of the three body parts. We measured maximum height, width, and length of head, prothorax, and the thoracoabdominal fusion and summed the volumes assuming cylindrically shaped body parts.

Tracheal Density of Cross-Sectional Areas. To determine tracheal investment in the head and the leg, we measured diameters of the major tracheal branches in x-ray images and calculated the cross-sectional area, assuming a circular cross-section of each tube. In the head, we compared the total cross-sectional area of the four major tracheae that branch from the mesothoracic spiracles into the head with the area of the orifice connecting the head capsule to the thorax (Fig. 1). In the leg, we compared the cross-sectional area of the leg trachea at the first leg segment (coxa) with the area of the leg orifice that opens into the body cavity (Figs. 1, 2, and 4; TrD_{leg}).

Species mean values with standard deviations of tracheal volume and cross-sectional areas of exoskeletal orifices and penetrating tracheae were plotted against body mass on a double-logarithmic plot to determine scaling patterns.

Phylogenetic Correction. Because species are related through evolution, their traits cannot be considered to be independent data points. To correct for phylogenetic relatedness, we used PIC analysis (23, 37) of the PDAP module, V. 1.08, in MESQUITE V. 1.12 (http://mesquiteproject.org and http://mesquiteproject.org/pdap_mesquite). In brief, PIC analysis calculates trait values of common ancestors as independent contrasts based on trait values and phylogenetic relationship of the examined species. The analysis requires the alignment of the investigated species on a phylogenetic tree. The branch lengths of the tree represent estimates of the variance in character evolution. To construct the phylogenetic tree of the four species of Tenebrionidae, we combined a cladistic analysis based on morphological characters up to the tribe level (figure 49, ref. 24) with a phylogenetic analysis of *T. molitor* and *T. castaneum* based on mitochondrial DNA (25). We combined both trees using normalized branch lengths (actual branch length divided by total tree length). Because of lack of phylogenetic data of the two *Eleodes* species, we set their branch lengths from tribe to species to one. This tree yielded the best standardization of independent contrasts (23) for the scaling analyses. To determine sensitivity to phylogenetic information, we repeated PIC with two additional trees of different structure, one with all branch lengths set to one (23) and another with branch lengths based on a different set of morphological characters (figure 51, ref. 24). Variation in branch lengths had only a small influence on scaling equations, and the results were not significantly different from the results obtained with the best fitting tree (Table 1 and SI Table 2 *A* and *B*).

Extrapolation of Body Length to Upper Limits of Tracheal Density. To determine the limits of tracheal investment on size, we plotted species mean values of tracheal density against body length (Fig. 4) and performed a SMA line-fit. We extrapolated the fitted line to assumed limits of tracheal densities. Tracheal density in the entire body was the tracheal volume density determined from the adapted stereological point-count method. Tracheal density in the leg orifice was calculated as the ratio between cross-sectional area of the trachea supplying the metathoracic leg and the penetrated leg orifice.

Statistics. Because all parameters are subject to equation errors rather than measurement errors (22), we used SMA (also known as reduced major axis) analysis to fit lines to allometric relationships (22, 38). With only four data points, we were not able to test for normal distribution, but SMA is less sensitive than ordinary least-square regression analysis to data that are not normally distributed or possess moderately different variances (22). SMA slope and its standard error, correlation coefficient (r), and coefficient of determination (r^2) were taken from the PDAP module. Intercept and confidence bands were calculated by applying standard equations (38, 39). We verified homogeneity of variance by plotting standardized residuals against standardized expected values (40). The tests justified the use of $\log_{10}$ transformed values for body-mass related allometries and the use of untransformed values for body-length related allometries. The statistical power of PIC analysis depends on the number of species and the magnitude of correlation between the characters (41). Although the number of species is small ($n = 4$), we obtained correlation coefficients >0.98 in all cases of body-mass-related allometries. This statistical power is larger than in a study with 15 species and a correlation coefficient of 0.5 between characters (41).

To compare different line-fit methods and the effect of PIC, we performed ordinary least-square (OLS) and SMA on phylogenetically uncorrected data. OLS regression was calculated in KyPlot 2 software beta 2 V.15 (Koichi Yoshioka, Tokyo, Japan); SMA was calculated in reduced major axis 1.17 software (42) by using 2,000 bootstrap iterations. Slopes of regression lines were compared with slopes calculated by best-fit PIC SMA and to theoretical values with Student's t test (38). Because of high correlation coefficients, the presented data are insensitive to the method of line fitting. (Table 1 and SI Table 2 *C–E*). Significance levels for all tests were set to $P = 0.05$.

We thank Theodore Garland, Jr., for support on the usage of PDAP and Michael LaBarbera and two anonymous reviewers for valuable comments on the manuscript. X-ray data were collected at the x-ray Science Division beamline 1-ID at the Advanced Photon Source, Argonne National Laboratory. Use of the Advanced Photon Source was supported by the U.S. Department of Energy, Office of Science, Office of Basic Energy Sciences, under Contract No. DE-AC02-06CH11357. This work was supported by National Science Foundation Grants 0419704 (to J.F.H.) and IBN-0344963 (to M.C.Q.).

1. Graham JB, Dudley R, Aguilar NM, Gans C (1995) *Nature* 375:117–120.
2. Dudley R (1998) *J Exp Biol* 201:1043–1050.
3. Shear W, Kukalová-Peck J (1990) *Can J Zool* 68:1807–1834.
4. Harrison JF, LaFreniere JJ, Greenlee KJ (2005) *Comp Biochem Physiol A* 141:372–380.
5. Gould SJ (1966) *Biol Rev* 41:587–640.
6. Kleiber M (1961) *The Fire of Life: An Introduction to Animal Energetics* (Wiley, New York).
7. Chown SL, Marais E, Terblanche JS, Klok CJ, Lighton JRB, Blackburn TM (2007) *Func Ecol* 21:282–290.
8. Pauly D (1998) *J Fish Biol* 53:1–17.
9. Palzenberger M, Pohla H (1992) *Rev Fish Biol Fisheries* 2:187–216.
10. Ultsch GR (1974) *Comp Biochem Physiol A* 47:485–498.
11. Pauly D (1998) *S Afr J Mar Sci* 20:47–58.
12. Lease HM, Wolf BO, Harrison JF (2006) *J Exp Biol* 209:3476–3483.
13. Hartung DK, Kirkton SD, Harrison JF (2004) *J Morph* 262:800–812.
14. Amy RWM, Bowes D, Burri PH, Haines J, Thurlbeck WM (1977) *J Anat* 124:131–151.
15. Vidic B, Burri PH (1973) *Anat Rec* 178:711–730.
16. Zeltner TB, Caduff JH, Gehr P, Pfenninger J, Burri PH (1987) *Resp Physiol* 67:247–267.
17. Weibel ER, Taylor CR, Hoppeler H (1991) *Proc Natl Acad Sci USA* 88:10357–10361.
18. Gehr P, Mwangi DK, Ammann A, Maloiy GMO, Taylor CR, Weibel ER (1981) *Resp Physiol* 44:61–86.
19. Taylor RE, Weibel ER, Weber J-M, Vock R, Hoppeler H, Roberts TJ, Brichon G (1996) *J Exp Biol* 199:1643–1649.
20. Socha JJ, Westneat MW, Harrison JF, Waters JS, Lee W-K (2007) *BMC Biology* 5:6.
21. Weibel ER (1979) *Stereological Methods. Vol 1. Practical Methods for Biological Morphometry* (Academic, London).
22. Warton DI, Wright IJ, Falster DS, Westoby M (2006) *Biol Rev* 81:259–291.
23. Garland T, Jr, Harvey PH, Ives AR (1992) *Syst Biol* 41:18–32.
24. Doyen JT, Tschinkel WR (1982) *Syst Entomol* 7:127–183.
25. Mestrovic N, Mravinac B, Plohl M, Ugarkovic D, Bruvo-Madaric B (2006) *Eur J Entomol* 103:709–715.
26. Rascón B, Harrison JF (2005) *J Ins Phys* 51:1193–1199.
27. Greenlee KJ, Nebeker C, Harrison JF (2007) *J Exp Biol* 210:1288–1296.
28. Kirkton SD, Niska JA, Harrison JF (2005) *J Exp Biol* 208:3003–3012.
29. Greenlee KJ, Harrison JF (2005) *J Exp Biol* 208:1385–1392.
30. Clarke KU (1957) *Proc R Entomol Soc London* 32:67–79.
31. Miller PL (1966) *J Exp Biol* 45:285–304.
32. Demoll R (1927) *Z Biol* 87:8–22.
33. Evans AV, Bellamy CL (2000) *An Inordinate Fondness for Beetles* (Univ of California Press, Berkeley).
34. Henry JR, Harrison JF (2004) *J Exp Biol* 207:3559–3567.
35. Jarecki J, Johnson E, Krasnow MA (1999) *Cell* 99:211–220.
36. Schmitz A, Perry SF (1999) *Physiol Biochem Zool* 72:205–218.
37. Felsenstein J (1985) *Am Nat* 125:1–15.
38. Zar JH (1999) *Biostatistical Analysis* (Prentice–Hall, Upper Saddle River, NJ).
39. Garland T, Jr, Ives AR (2000) *Am Nat* 155:3.
40. Osborne JW, Waters E (2002) *Pract Assessment Res Eval* 8 http://pareonline.net/getvn.asp?v=8&n=2.
41. Garland T, Jr, Adolph SC (1994) *Physiol Zool* 67:797–828.
42. Bohanak A, Van der Linde K (2004) www.kimvdlinde.com/professional/rma.html.